2012

The Li-8(p, alpha)He-5 reaction at low energies, and Be-9 spectroscopy around the proton threshold

PHYSICAL REVIEW C, COLLEGE PK, v. 86, n. 6, pp. 932-939, DEC 26, 2012

The ^{8}Li$(p,\alpha)^{5}$He reaction at low energies, and ^{9}Be spectroscopy around the proton threshold

D. R. Mendes, Jr.,[1] A. Lépine-Szily,[1] P. Descouvemont,[2] R. Lichtenthäler,[1] V. Guimarães,[1] P. N. de Faria,[1] A. Barioni,[1] K. C. C. Pires,[1] V. Morcelle,[1] R. Pampa Condori,[1] M. C. Morais,[1] E. Leistenschneider,[1] C. E. F. Lima,[1] J. C. Zamora,[1] J. A. Alcantara,[1] V. Zagatto,[1] M. Assunção,[3] and J. M. B. Shorto[4]

[1]*Departamento de Física Nuclear, Instituto de Física da Universidade de São Paulo, Caixa Postal 66318, 05315-970, São Paulo, SP, Brazil*

[2]*Physique Nucléaire Théorique et Physique Mathématique, C.P. 229, Université Libre de Bruxelles (ULB), B-1050 Brussels, Belgium*

[3]*Departamento de Ciências Exatas e da Terra, Universidade Federal de São Paulo, Campus Diadema, São Paulo, SP, Brazil*

[4]*Instituto de Pesquisas Energéticas e Nucleares (IPEN-CNEN), Comissão Nacional de Energia Nuclear, São Paulo, SP, Brazil*

(Received 14 February 2012; revised manuscript received 14 September 2012; published 26 December 2012)

We present a direct measurement of the low-energy ^{8}Li$(p,\alpha)^{5}$He cross section, using a radioactive ^{8}Li beam impinging on a thick target. With four beam energies, we cover the energy range between $E_{\text{c.m.}} = 0.2$ and 2.1 MeV. An R-matrix analysis of the data is performed and suggests the existence of two broad overlapping resonances ($5/2^{+}$ at $E_{\text{c.m.}} = 1.69$ MeV and $7/2^{+}$ at $E_{\text{c.m.}} = 1.76$ MeV). At low energies our data are sensitive to the properties of a subthreshold state ($E_x = 16.67$ MeV) and of two resonances above threshold. These resonances were observed in previous experiments. The R-matrix fit confirms spin assignments, and provides partial widths. We propose a new ^{8}Li$(p,\alpha)^{5}$He reaction rate and briefly discuss its influence in nuclear astrophysics.

DOI: 10.1103/PhysRevC.86.064321 PACS number(s): 21.10.Hw, 21.10.Tg, 25.40.Hs, 27.20.+n

I. INTRODUCTION

The availability of radioactive beams provides new opportunities in nuclear physics [1]. On the one hand, recent experiments involving radioactive beams have been very successful in nuclear astrophysics [2], where many stellar scenarios involve short-lived nuclei [3]. On the other hand, radioactive beams provide a probe of the nuclear structure in unusual conditions of excitation energy and isospin. Many experiments have been performed with various beams such as ^{6}He or ^{11}Li (see references in Ref. [1]). At energies near the Coulomb barrier or above, these experiments provide valuable information on the structure of exotic nuclei.

In this work, we present a measurement of the ^{1}H$(^{8}$Li$,\alpha)^{5}$He cross section at low energies. This experiment has been performed at Radioactive Ion Beams in Brazil (RIBRAS) [4,5] with a ^{8}Li beam ($\tau_{1/2} \approx 0.8$ s). One of our goals is to investigate the ^{9}Be structure near the proton threshold (16.89 MeV) through the ^{8}Li$(p,\alpha)^{5}$He reaction. The ^{9}Be level scheme is well known at low excitation energies [6,7], but the high-energy region is still uncertain. The ^{1}H$(^{8}$Li$,\alpha)^{5}$He reaction allows the precise determination of several resonance parameters: energies, spins, and proton and α widths. A transfer reaction offers several advantages. In particular, the isospin of the exit channel limits the population to $T = 1/2$ states in ^{9}Be, and interferences with the Coulomb interaction, which are dominant in elastic-scattering experiments, are absent in a transfer reaction.

Our experiment also addresses some issues for stellar models. Reactions associated with ^{8}Li play a role in nuclear astrophysics [8]. In particular the ^{8}Li$(\alpha,n)^{11}$B reaction is expected to affect nonstandard Big Bang nucleosynthesis (see Ref. [9] and references therein) and has been investigated by various groups (see, for example, Ref. [10] and references therein). More recently, it was suggested that this reaction could also affect r-process nucleosynthesis [11]. Consequently, the role of other reactions involving ^{8}Li is an important issue which is addressed by the present experiment. The ^{8}Li$(p,\alpha)^{5}$He cross section was measured at a single energy (1.5 MeV) about twenty years ago [12]. Here we provide the experimental cross section over a wide energy range (from 0.2 to 2.1 MeV), which allows us to determine a more reliable reaction rate.

The paper is organized as follows. In Sec. II, we present the experimental setup and the conditions of the experiment. Section III is devoted to an R-matrix analysis of the data and to a discussion of ^{9}Be spectroscopy near the proton threshold. We briefly discuss the associated reaction rate. Concluding remarks and outlook are presented in Sec. IV.

II. EXPERIMENTAL METHOD AND RESULTS

A. Experimental setup

The ^{1}H$(^{8}$Li$,\alpha)^{5}$He reaction was studied with the RIBRAS facility, installed at the 8-UD Pelletron Tandem of the University of São Paulo. The use of a ^{8}Li beam hitting the hydrogen atoms of a $(CH_2)_n$ plastic target, in inverse kinematics, made it possible to reach low energies in the center-of-mass reference frame. We give here a short description of the experimental equipment; more detail can be found in Refs. [4,5]. This facility consists of two superconducting solenoids with a 6.5-T maximum central magnetic field and a 30-cm clear warm bore. The ^{7}Li^{3+} primary beam was accelerated by the Pelletron Accelerator at energies between 16 and 22 MeV and the beam current was typically 300 nA. The ^{8}Li^{3+} beam was produced by the ^{9}Be$(^{7}$Li,^{8}Li$)^{8}$Be transfer reaction ($Q = 0.367$ MeV) and focused by the first solenoid onto the secondary target. In this work we have used a ^{9}Be foil of 16 μm thickness as the production target. A tungsten stopper located behind the Be foil measured and integrated the primary beam current. The stopper and a collimator at the entrance of the solenoid bore defined the angular acceptance of the system; the angles of the secondary ^{8}Li beam with respect to the magnetic field in the solenoid (our z axis) varied between, respectively, 2°–6° at the entrance and 1.5°–4.5° at the exit of the solenoid.

The solenoid selected and focused the chosen radioactive beam onto the secondary target, located in a scattering chamber between the two solenoids. The ^{8}Li production rate was maximized at each energy by varying the solenoid current and measured through Rutherford elastic scattering on a ^{197}Au secondary target. The measurement with the gold target was performed frequently and the production rate was quite constant at each energy but depended on the incident energy, varying between 10^5 and 5×10^5 particles per second at the secondary target position.

The secondary targets were made of a $(CH_2)_n$ polyethylene foil of 6.8 mg/cm^2 thickness and a gold target of 5 mg/cm^2 thickness. The $(CH_2)_n$ target thickness was less than the range of the ^{8}Li beam for the highest incident energy. Due to the high Q value of the reaction ($+14.42$ MeV), the α particles presented a high kinetic energy and were detected at forward angles using four ΔE-E Si telescopes, where the ΔE and E detectors had thicknesses of 20 and 1000 μm, respectively, with geometrical solid angles of 18 msr. The effective solid angles, the total angular uncertainty (full width at half maximum $= 5.1^\circ$), and the average detection angles were determined by using a Monte Carlo simulation, which took into account the collimator size, the secondary beam spot size ($\phi = 4$ mm), the secondary beam divergence, and the angular distribution at forward angles.

We have used a primary $^{7}Li^{3+}$ beam at four incident energies: 16.3, 17.4, 19.5, and 21.6 MeV, which have produced ^{8}Li secondary beams with energies of 13.2 ± 0.3, 14.5 ± 0.3, 17.0 ± 0.4, and 19.0 ± 0.4 MeV impinging on the thick $(CH_2)_n$ secondary target. The solenoid performed a magnetic rigidity selection and determined the secondary beam energies, which were also confirmed by the energy measurement in the Si telescopes using the gold target. Other ions with the same magnetic rigidity but different charges, masses, and energies could also be focused together with the $^{8}Li^{3+}$ ions ($\geqslant$50%). The degraded primary $^{7}Li^{2+}$ beam, with a lower charge state and with much lower energy ($\leqslant$30%), α particles ($\sim$15%), protons, deuterons, and tritons ($\leqslant$5%) were the most intense contaminant beams. The Si detectors were energy calibrated with the α particles of an ^{241}Am source and using the ^{8}Li and contaminant beams scattered on the gold target at several detection angles.

In Fig. 1 we present the bidimensional energy spectra of the scattered ^{8}Li and contaminant beams obtained with $E(^{8}\text{Li}) = 19.0$ MeV, the detector at $13.5^\circ \pm 2.6^\circ$, and gold [Fig. 1(a)] or $(CH_2)_n$ [Fig. 1(b)] secondary targets.

In Fig. 1(b), one can observe the region of α particles, also called the "α-strip," where a strong peak at $E_{\text{total}} = E_\alpha = 15$ MeV is observed. Energetically, this peak can be due to $^{12}\text{C}(\alpha, \alpha)^{12}\text{C}$ elastic scattering of the contaminant α beam on the carbon content of the $(CH_2)_n$ secondary target.

The tail of α particles ranging from this peak to $E_{\text{total}} = E_\alpha = 32$ MeV contains the α particles of the $^{1}\text{H}(^{8}\text{Li}, \alpha)^{5}\text{He}$ reaction, which has a large positive Q value. In Fig. 1(c) we present the projection of the α-strip on the total energy axis, which reveals a dominant peak around $E_{\text{total}} = E_\alpha = 27$ MeV, suggesting a broad resonance in ^{9}Be, with an excitation energy around 18.6 MeV ($E_{\text{c.m.}} = 1.7$ MeV).

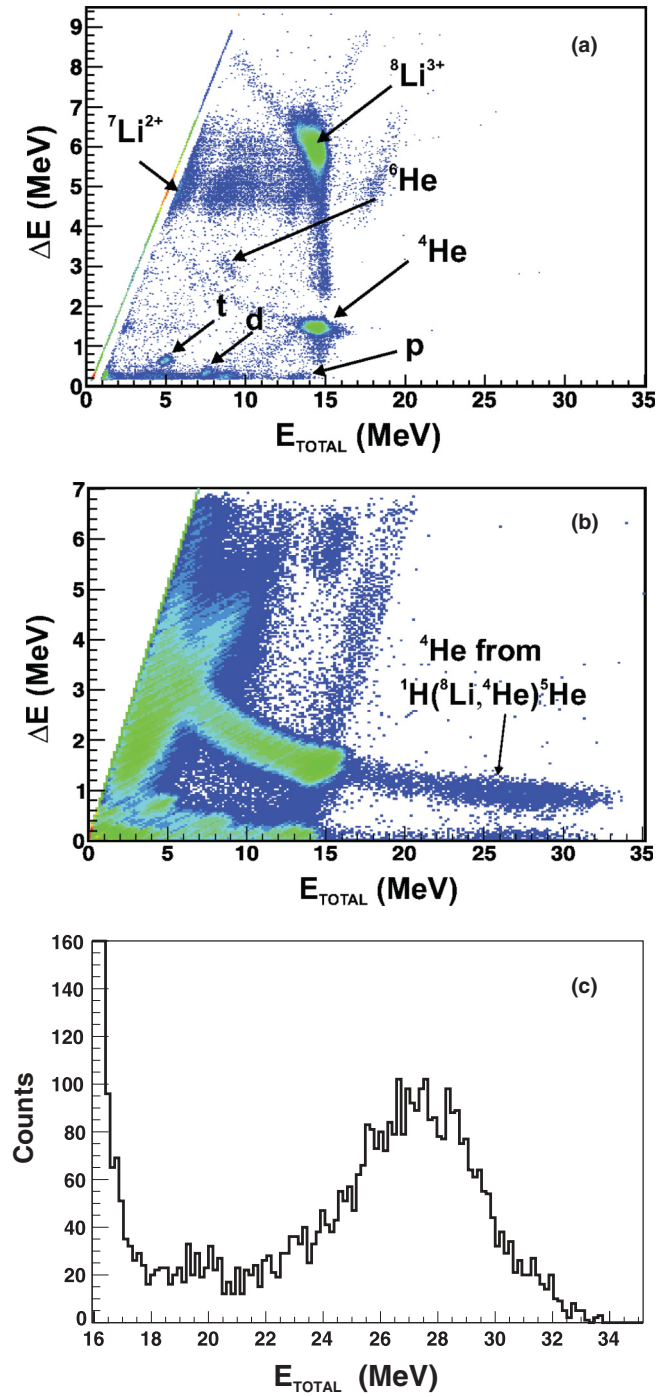

FIG. 1. (Color online) Bidimensional energy spectra obtained at $E_{\text{lab}}(^{8}\text{Li}) = 19.0$ MeV and $\theta_{\text{lab}} = 13.5^\circ \pm 2.6^\circ$, with the scattered ejectiles of all beams focused by the first solenoid, respectively, on the gold (a) or on the $(CH_2)_n$ (b) secondary targets. The abscissa is the total energy in MeV and the ordinate is the energy loss in the ΔE detector in MeV. (c) The projection of the α-strip on the total energy axis.

B. Thick-target method and identification of the production mechanism of the α particles

Due to the high proton threshold in ^{9}Be (16.8882 MeV), even at low incident energies used in this experiment, the

TABLE I. Available experimental data on ^{9}Be states near the ^{8}Li + p threshold (16.8882 MeV; see Ref. [13]). Energies E_r and E_x are expressed in MeV, and total widths Γ are in keV.

E_r	E_x	$J^\pi; T$	Γ
−0.92	15.97	$T = 1/2$	≈300
−0.217	16.671	$(5/2^+); 1/2$	41 ± 4
0.0870	16.9752	$1/2^-; 3/2$	0.389 ± 0.010[a]
0.410	17.298	$(5/2)^-$	200
0.605	17.493	$(7/2)^+; 1/2$	47
1.13	18.02		
1.69	18.58		
1.762	18.650	$(5/2^-; 3/2)$	300 ± 100
2.31	19.20		310 ± 80
2.53	19.42		600 ± 300

[a]$\Gamma_p = 12^{+12}_{-6}$ eV; $\Gamma_\alpha + \Gamma_n = 290 \pm 20$ eV [14].

^{1}H(^{8}Li, α)^{5}He reaction can populate the ^{9}Be compound nucleus at high excitation energies, where the nucleus is unbound and presents several poorly known resonances [13]. In particular, the partial widths, which determine the cross section at low energies, are not available. The existing data are given in Table I.

The maximum incident energy in the laboratory frame was $E(^8\text{Li}) = 19.0 \pm 0.4$ MeV, which corresponds to $E_{\text{c.m.}} = 2.11 \pm 0.04$ MeV for the $p + ^8$Li system; thus all resonances in ^{9}Be below $E_{\text{c.m.}} = 2.15$ MeV could be populated in the thick target, while the ^{8}Li projectile is slowing down. Whenever a resonance is populated, a larger number of α particles can be produced and detected in the Si telescopes, producing a peak in the α-energy spectrum. Thus, the energy spectrum of the α particles will represent the excitation function of the reaction, and peaks in the energy spectrum correspond to resonances in the excitation function.

However, by taking into account the experimental thresholds, the detected α particles can originate from the $\alpha + ^5$He channel as well as from the $^8\text{Be} + n$ channel. In the ^{1}H(^{8}Li, α)^{5}He reaction, the recoiling ^{5}He is unbound and disintegrates into an α particle and a neutron. Similarly, in the ^{1}H(^{8}Li, ^{8}Be)n reaction the ^{8}Be is unbound and breaks into two α particles. We considered each reaction to occur in two steps, each one being a two-body reaction. We have used kinematic arguments to identify the reaction mechanism of the α particles belonging to the broad peak at $E_\alpha = 27$ MeV. At the highest beam energy $E(^8\text{Li}) = 19.0$ MeV, we have performed measurements at several angles, between $\theta_{\text{lab}} = 10.5^\circ$ and 46.5°. In Fig. 2, we present the energy centroids of this peak [see Fig. 1(c)] as a function of the laboratory detection angles (dots). We compared these points to several kinematic calculations. The solid line uses the reaction ^{1}H(^{8}Li, α)^{5}He at a well-defined resonance at $E_{\text{c.m.}} = 1.7$ MeV, which corresponds to $E(^8\text{Li}) = 15.3$ MeV ($E_{\text{c.m.}} = E_{\text{lab}} \frac{M_{\text{target}}}{M_{\text{proj}}+M_{\text{target}}} \sim E_{\text{lab}}/9$), and it agrees very well with the experimental points, indicating that the broad peak corresponds to the ^{1}H(^{8}Li, α)^{5}He reaction.

However, if the recoiling ^{5}He would be excited ($E^* = 1.27$ MeV, $\Gamma \sim 6$ MeV) the kinetic energy of the ejected α particle would be smaller but its kinematic locus could overlap the ground-state locus. Thus the broad peak is due to the two-body ^{1}H(^{8}Li, α)^{5}He reaction leaving the recoiling ^{5}He in its ground or excited state.

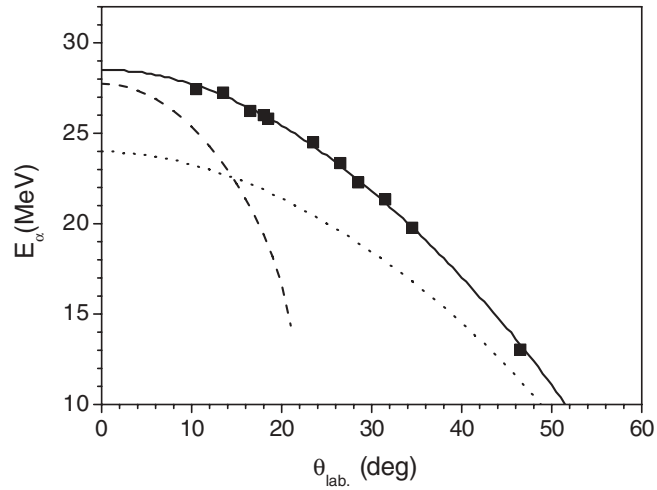

FIG. 2. Energy centroids of the peak at $E_\alpha = 27$ MeV as a function of the laboratory detection angles (dots) measured at $E(^8\text{Li}) = 19.0$ MeV. The angular uncertainty is ±2.6°. The solid line describes the kinematic variation of the reaction ^{1}H(^{8}Li, α)^{5}He at $E(^8\text{Li}) = 19.0$ MeV. The dashed line corresponds to the energy of the ^{8}Be from the ^{1}H(^{8}Li,^{8}Be)n reaction at $E(^8\text{Li}) = 19.0$ MeV; the α particles originating from the decay of ^{8}Be have energy typically about half of the ^{8}Be energy. The dotted line corresponds to the ^{1}H(^{7}Li, α)^{4}He reaction at $E(^7\text{Li}^{2+}) = 9.66$ MeV.

The dashed line corresponds to the kinematic behavior of the ^{8}Be nucleus formed in the ^{1}H(^{8}Li,^{8}Be)n reaction. The α particles originating from the decay of ^{8}Be have not a single kinematic locus and for this reason were not plotted on Fig. 2, but their energy is typically half of the ^{8}Be energy, i.e., between 10 and 13 MeV for $E(^8\text{Li}) = 19.0$ MeV for forward detection angles, and thus they are in complete disagreement with the data.

The direct $^4\text{He} + ^4\text{He} + n$ three-body breakup, which contributes to the background, will be discussed in Sec. II E. The α particles could also come from reactions induced by the degraded primary $^7\text{Li}^{2+}$ beam, such as the ^{12}C(^{7}Li, α)^{15}N and ^{1}H(^{7}Li, α)^{4}He reactions. For the ^{12}C(^{7}Li, α)^{15}N reaction, even the most energetic α particles have energies lower ($E_\alpha = 19.5$ MeV) than the broad peak observed at $E_\alpha = 27$ MeV. Concerning the ^{1}H(^{7}Li, α)^{4}He reaction, the kinematic calculation shown in Fig. 2 (dotted line) is not consistent with the experimental points.

C. Contamination in the target and contaminant beams

The α-energy spectrum of Fig. 1(c) is covered by contributions from other contaminant reactions for $E_\alpha \leqslant 18$ MeV. In order to be able to observe the α particles from the reaction ^{1}H(^{8}Li, α)^{5}He for lower α energies we decreased the incident ^{8}Li energy, the solenoid magnetic rigidity, and consequently the energy of the contaminant beams. The purpose of using four different ^{8}Li beam energies was to study the reaction

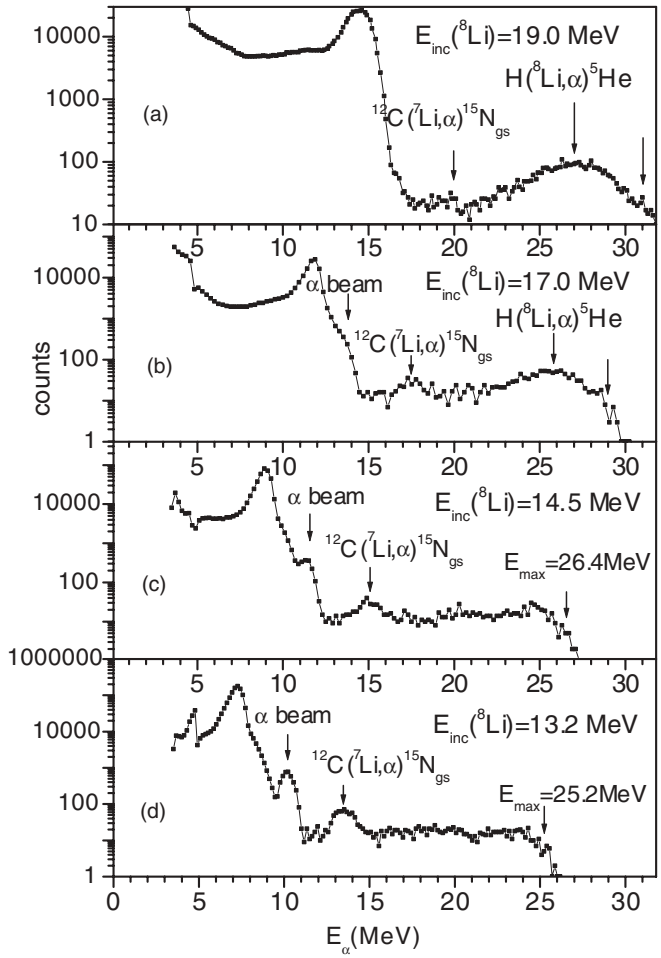

FIG. 3. Energy spectra of the α particles measured with a ^{8}Li beam (and contaminants) on the $(CH_2)_n$ thick target at $\theta_{lab} = 13.5^{\circ} \pm 2.6^{\circ}$ and $E_{inc}(^{8}Li) = 13.2$, 14.5, 17.0, and 19.0 MeV. Some arrows indicate peaks, which have a rapid variation with the incident energy and cannot be related to resonances in the compound systems; others indicate the maximum energy of α particles from the $^{1}H(^{8}Li, \alpha)$ reaction, with the energy loss in the target taken into account.

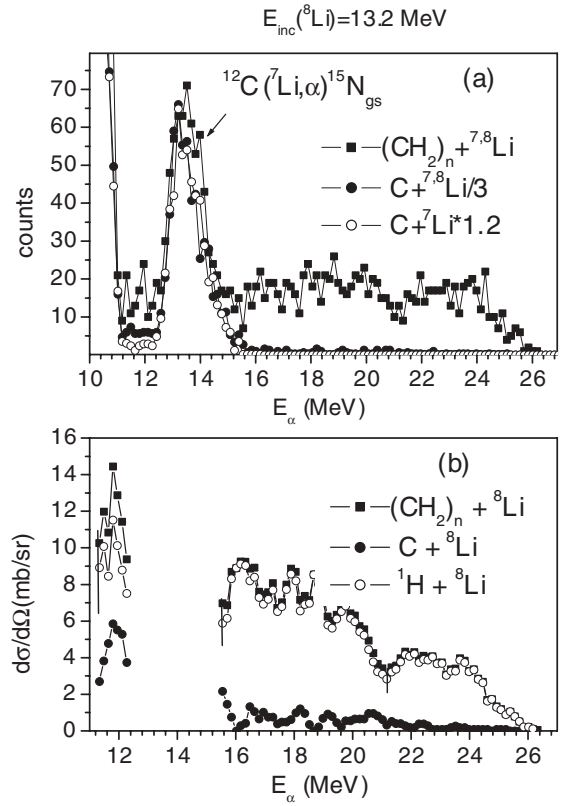

FIG. 4. (a) Comparison of three different excitation functions measured at 13.2 MeV incident energy, one measured with $(CH_2)_n$ and the other two with a natural carbon target. The excitation functions were normalized to superimpose the peak at $E_\alpha = 13.5$ MeV, which corresponds to the $^{12}C(^{7}Li, \alpha)^{15}N_{gs}$ reaction, present in all three excitation functions. (b) Comparison of the cross sections of the $(^{8}Li, \alpha)$ reaction produced on $(CH_2)_n$ and on natural carbon targets and the result of the subtraction.

of interest in different excitation energy regions of the ^{9}Be compound nucleus.

In Fig. 3 we present the excitation functions measured at four incident energies. At lower incident energies the peak at $E_\alpha = 27$ MeV disappears and other peaks appear. These new peaks shift with incident energy and are therefore not due to resonances in any of the compound systems. They were identified by their energy and kinematic variations as arising from the reactions $^{12}C(^{7}Li, \alpha)^{15}N_{gs}$ and $^{12}C(\alpha, \alpha)^{12}C$ and a peak due to the contaminant α beam, which hits the detector without traversing any target.

In order to subtract the contribution of reactions on the natural carbon present in the $(CH_2)_n$ target, we have performed measurements at the same four energies using a thick natural carbon target (15 mg/cm^2) and a ^{8}Li beam with its α particle and $^{7}Li^{2+}$ contaminations. The low-energy peaks were still in the spectra, proving that they are not due to reactions on the hydrogen content of the $(CH_2)_n$ target. We also performed measurements without the ^{8}Li beam, with only α particle and $^{7}Li^{2+}$ contaminant beams, on both $(CH_2)_n$ and natural carbon targets. We realized this by reducing the primary beam energy without changing the magnetic field in the solenoid; thus the monoenergetic ^{8}Li beam was no longer focused, but the degraded primary beam and the α particles were still focused with the same energy. Performing these measurements on natural carbon target confirmed that the $^{12}C(^{7}Li, \alpha)^{15}N_{gs}$ reaction was responsible for the peaks identified in Fig. 3. They are well-defined peaks because the low-energy ^{7}Li ions stop close to the entrance of the target foil.

In Fig. 4(a) we compare three different excitation functions measured at 13.2 MeV incident energy, one measured with $(CH_2)_n$ and the other two with natural carbon. We show data at 13.2 MeV, where the peak at $E_\alpha = 13.5$ MeV, used for normalization purpose, is the largest. However, the procedure described here will be the same at other incident energies also.

These excitation functions are the result of a smoothing procedure, using adjacent averaging of three channels, since every channel corresponds to 150 keV and the experimental resolution at low α energies is 450 keV, increasing to 670 keV at the highest energies. The excitation functions were normalized by the peak area at $E_\alpha = 13.5$ MeV, which cor-

responds to the ^{12}C(^{7}Li, α)^{15}N$_{gs}$ reaction, present in all three excitation functions. The normalization of the three excitation functions has allowed the subtraction of the contributions of the contaminant ^{7}Li beam and the natural carbon content of the target from the energy spectra obtained with ^{7,8}Li beams on the natural carbon and $(CH_2)_n$ targets.

As can be seen in Fig. 4(a) this peak shape differed with the targets; thus the peak region was excluded from the subtraction to prevent large oscillations in the subtracted yield. The slowly varying yield above and below the peak allows for a subtraction which is not affected by the peak shape difference. From the subtracted energy spectra for $(CH_2)_n$ + ^{8}Li and ^{12,13}C + ^{8}Li systems, we can calculate the cross sections of the (^{8}Li, α) reaction produced on CH_2 and natural carbon targets. The main source of the experimental uncertainty was the statistical error, which was propagated in the calculations, such as normalizations, subtractions, etc.

In Fig. 4(b) we compare these cross sections and the result of their subtraction. The cross section of the (^{8}Li, α) reactions on natural carbon (thus containing ^{12}C + ^{13}C) is only important in the low-energy region as it drops to low values at the higher energy region. This behavior is similar at the higher incident energies also. The experimental error for the final cross section is only shown at three typical points. The ^{12}C(^{7}Li, α)N$_{gs}$ peak, which moves with incident energy, produces a gap in all excitation functions. However, the measurement at four energies has allowed an almost complete coverage of α energies from 11 to 31 MeV.

D. Conversion from laboratory to center-of-mass frame and cross-section calculations using a thick target

The α-particle kinetic energy is a function of the ^{8}Li kinetic energy. The corresponding ^{8}Li energy was found through the following method: the thick target was divided into thin slices of 0.1 mg/cm^2, the energy of the ^{8}Li beam at the end of each slice was calculated by subtracting the energy loss from the incident energy, then the energy of the emitted α particle was obtained from the kinematics of the ^{1}H(^{8}Li, α)^{5}He reaction, followed by the energy loss calculation of the α particles in the rest of the target, by taking into account the detection angle. This calculation yielded the correspondence between α-particle energy and ^{8}Li energy, as a function of the angle and incident energy. The center-of-mass energy of the ^{8}Li + p system can be easily calculated from the ^{8}Li laboratory energy, through $E_{\mathrm{c.m.}} = E_{\mathrm{lab}} \frac{M_{\mathrm{target}}}{M_{\mathrm{proj}}+M_{\mathrm{target}}}$.

The differential cross section in the center-of-mass frame is calculated using

$$\frac{d\sigma}{d\Omega}(E,\theta)_{\mathrm{c.m.}} = \frac{N \frac{dE_{8_{Li}}}{dE_{\alpha}} J \frac{dE}{dx}}{\Delta\Omega N_{\mathrm{inc}} \Delta E(^{8}\mathrm{Li})}, \quad (1)$$

where N is the total number of α particles detected with energy corresponding to the interval E and $E + \Delta E(^{8}$Li), the derivative $\frac{dE_{8_{Li}}}{dE_{\alpha}}$ multiplies the yield due to the conversion from α-particle energy to ^{8}Li energy, $\Delta\Omega$ is the solid angle of the detector considered, N_{inc} is the number of ^{8}Li ions incident on the secondary target, J is the Jacobian that converts the geometrical solid angle from the laboratory frame to the center-of-mass frame, and N_{target} is the number of target atoms per unit area, which is not constant, since the energy loss of the beam, $\Delta E(^{8}$Li) per unit distance Δx, depends on the energy. This provides

$$N_{\mathrm{target}} = \frac{\Delta E(^{8}\mathrm{Li})}{\frac{dE}{dx}}, \quad (2)$$

where $\Delta E(^{8}$Li) is the energy step of the spectrum in $E_{\mathrm{lab}}(^{8}$Li), and $\frac{dE}{dx}$ is the stopping power of ^{8}Li in the thick $(CH_2)_n$ target. The energy variations of the stopping power $\frac{dE}{dx}$, of the derivative $\frac{dE_{8_{Li}}}{dE_{\alpha}}$, and of the Jacobian were fitted with polynomials and taken into account in the calculation of the differential cross sections.

E. Background considerations: three-body and sequential decays

The simultaneous breakup into three or more particles during the ^{1}H + ^{8}Li collision produces a continuous background in the excitation function. The energy balance shows that only the breakup into three particles, namely, into ^{4}He + ^{4}He + n can occur. The phase-space model (PSM) developed by Fermi [15] computes statistically the probability of creation of an α particle with a given energy distribution. The continuous energy distributions of α particles resulting from the three-body breakup depend on the Q value of the reaction, on the masses of the nuclei involved, and on the incident energy. Thus, we integrated the yield over the decreasing incident energy in the thick target to obtain the final energy distribution. Its normalization was limited by the constraint that the sum of backgrounds should not be higher than the experimental cross section.

Because of the sequential reaction ^{1}H(^{8}Li, α)^{5}He the α particles coming from the decay of ^{5}He would also contribute to the background. A Monte Carlo simulation was performed: it included the slowing down of ^{8}Li in the $(CH_2)_n$ target and the reaction probability described by a Breit-Wigner (BW) shape, a resonance located at $E(^{8}\mathrm{Li}) = 15.3$ MeV with $\Gamma = 0.7$ MeV. From Fig. 2, we observe a resonance at $E_{\mathrm{c.m.}} = 1.7$ MeV, which corresponds to $E(^{8}\mathrm{Li}) \sim E_{\mathrm{c.m.}} \times 9 = 15.3$ MeV. The width Γ was determined by comparing the data with calculations using different widths values of 0.6, 0.7, 0.8, and 0.9 MeV and choosing the best agreement with the data. The sequential three-body kinematics calculated the angle and energy of the "direct" α particles coming from the first step and was followed by the decay of the recoiling ^{5}He, where again the angle and energy of the "decay" α particles was calculated. Only the α particles hitting the detector were counted. Finally, the energy loss of the α particles in the remaining part of the target was calculated. The result of the calculation was that the energy-integrated cross section for "direct" alpha and "decay" α emission were about the same: 50% each.

We also took into account the possible excitation of ^{5}He, using its excitation energy and width ($E^* = 1.27$ MeV and $\Gamma = 6$ MeV) given in the literature [13]. The energy spectrum of the α particles coming from the decay of the excited ^{5}He is

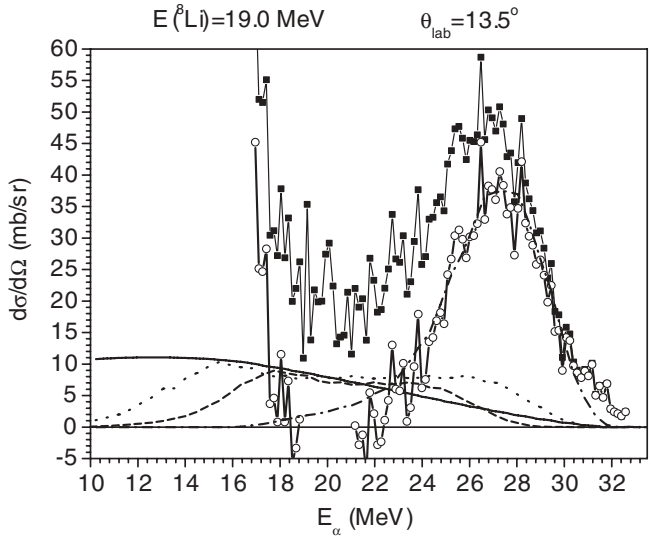

FIG. 5. The experimental cross sections measured at $E(^8\mathrm{Li}) = 19.0$ MeV (line with squares) compared to the continuous energy distribution of the α particles resulting from the three-body breakup (solid line) and to the energy spectra of the α particles resulting, respectively, from the decay of $^5\mathrm{He}_{\mathrm{g.s.}}$ (dashed line) and of $^5\mathrm{He}^*$ (dotted line). The simulation assumes a Breit-Wigner resonance situated at $E(^8\mathrm{Li}) = 15.3$ MeV with $\Gamma = 0.7$ MeV (dash-dotted line). The cross section obtained after the subtraction of all three background contributions is represented by circles. The error bars are omitted for the sake of clarity.

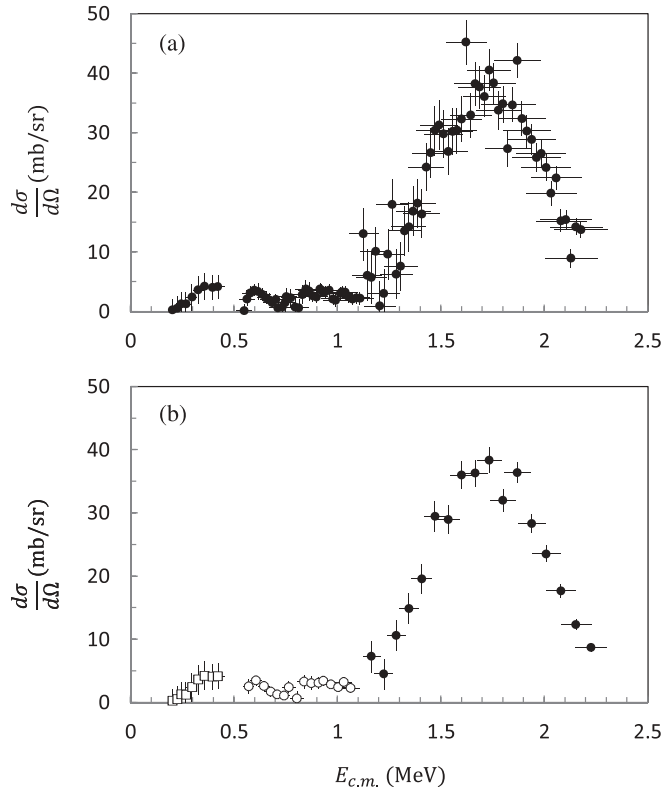

FIG. 6. Complete excitation function at $\theta_{\mathrm{lab}} = 13.5^\circ$ without an averaging procedure (a) and with an averaging procedure (b). See text for details.

broader, reaching energies higher than those coming from the ground state. In this calculation, the sum of "decay" α particles (52%) is similar to that of the direct process, represented by the Breit-Wigner peak (48%). Since the Breit-Wigner formula corresponds to a cross section in the center-of-mass frame, the result of the simulation has to be compared to and subtracted from the cross section [see Eq. (1)]. Quite large variations were performed in the relative proportion (from 30% to 70%) between decay from ground state and excited state in ^{5}He, with the effect on the final result being much smaller than the total uncertainty of the subtracted cross section.

In Fig. 5, the experimental cross sections measured at $E(^8\mathrm{Li}) = 19.0$ MeV (line with squares) are compared to the continuous energy distribution of the α particles resulting from the three-body breakup (solid line) and to the energy spectra of the α particles resulting, respectively, from the decay of $^5\mathrm{He}_{\mathrm{g.s.}}$ (dashed line) and of $^5\mathrm{He}^*$ (dotted line). The direct α spectrum is described by the Breit-Wigner resonance located at $E(^8\mathrm{Li}) = 15.3$ MeV with $\Gamma = 0.7$ MeV (dash-dotted line). The cross section obtained after the subtraction of all three background contributions (represented by circles) is in excellent agreement with the "direct" α simulation. The final error bars after the subtraction were calculated by assuming 30% error in each subtracted background and summing quadratically each term with the statistical error. For the excitation function at $E(^8\mathrm{Li}) = 17.0$ MeV, the same procedures were adopted as described in detail above. At $E(^8\mathrm{Li}) = 13.2$ and 14.5 MeV the low-energy resonances are observed at $E_{\mathrm{c.m.}} = 0.4$ and 0.6 MeV and the same procedures were adopted as described above for the $E_{\mathrm{c.m.}} = 1.7$ MeV resonance (see Fig. 5).

The complete excitation function is composed of the excitation functions measured at four beam energies and is shown in Fig. 6(a). After the subtraction of the contribution of reactions on natural carbon and contaminant beams, and the contribution coming from the decay of ^{5}He and breakup into $\alpha + \alpha + n$ it corresponds only to the $^1\mathrm{H}(^8\mathrm{Li}, \alpha)^5\mathrm{He}$ reaction at any energy region.

The energy resolution for the $^1\mathrm{H}(^8\mathrm{Li}, \alpha)^5\mathrm{He}$ reaction contains two components: the energy resolution of the ^{8}Li beam (measured by the experimental width of the peak of the elastically scattered ^{8}Li on the ^{197}Au target) and the calculated kinematic broadening, in which the angular aperture of the detector, the angular straggling in the target, the angular divergence of the secondary beam, and the kinematics of the reaction $^1\mathrm{H}(^8\mathrm{Li}, \alpha)^5\mathrm{He}$ are considered. The first term is almost constant and the second is almost linear with energy, having a slight quadratic term. The second term could not be verified experimentally but the kinematic calculations are reliable. The two components were summed quadratically and were approximated by an energy resolution that varied linearly from 20 keV in the low-energy region to 100 keV at the maximum energy in the center-of-mass frame.

In the lower panel of Fig. 6, an averaging procedure has been applied. The data at 19.0 MeV (solid circles) are presented after averages over three consecutive energies. In the intermediate region [open circles, corresponding to $E(^8\mathrm{Li}) = 17.0$ MeV]

we average over two energies, while no averaging procedure is applied to low-energy data [open squares, corresponding to $E(^8\text{Li}) = 13.2$ and 14.5 MeV]. In Fig. 6, two peaks can be clearly observed at $E_{\text{c.m.}} \sim 0.4$ and 0.6 MeV. These resonances are known in the literature (see Table I) and will be discussed in more detail in the next section.

F. Comparison with previous results

The ^{1}H(^{8}Li, α)^{5}He reaction was previously measured [12], using a ^{8}Li beam on thin $^{13}CH_2$ or $C_3H_6N_6$ (melamine) targets with ΔE-E telescopes. The authors measured an angular distribution at a fixed energy and their differential cross section at $\theta_{\text{lab}} = 12.5^\circ$ was about 12 ± 5 mb/sr, which is apparently lower than our value by a factor of 2. They claim that $E_{\text{c.m.}}$ was 1.5 MeV. However, we found inconsistencies in this work between the incident energy (quoted as 14.6 MeV in the text and 14 MeV in Fig. 1), the target thicknesses quoted in the text, and the α-particle energies indicated on the calibrated energy spectra of Fig. 1. The calculated α-energy, with the energy loss of the incident ^{8}Li and the emerging α particles taken into account, should be ~1.5–2 MeV higher than indicated on Fig. 1.

In order to correct those problems, either the incident energy has to be lower or the targets have to be thicker. If we suppose an incident energy of 14 MeV for a melamine target with double thickness we obtain the correct α energy (25.5 MeV). Consequently, the center-of-mass energy in the center of the thin target will be 1.4 MeV instead of 1.5 MeV. In our experiment, where the complete excitation function was measured, at $E_{\text{c.m.}} = 1.41 \pm 0.09$ MeV we measured a cross section of 16 ± 4 mb/sr, and this is therefore consistent with Ref. [12].

III. *R*-MATRIX ANALYSIS OF THE DATA

A. General formalism

The experimental cross sections of Fig. 6 are fitted by an R-matrix parametrization [16,17]. This formalism is based on a division of the space into two regions: an internal region (of radius a) where the nuclear interaction is dominant and where the physics of the problem is described by a set of real, energy-independent parameters and the external region where the colliding nuclei interact by the Coulomb force only. For physical parameter sets, the cross sections are nearly independent of the channel radius a.

In a given partial wave, with total spin J and parity π, the R matrix depends on energy and is defined as

$$R_{ij}(E) = \sum_{\lambda=1}^{N} \frac{\gamma_i^\lambda \gamma_j^\lambda}{E_\lambda - E}, \tag{3}$$

where i and j represent the entrance and exit channels (and for the sake of clarity we do not write the quantum numbers $J\pi$). Each channel is characterized by the masses and charges, the channel spin I, and the relative angular momentum ℓ. The N poles λ in partial wave $J\pi$ correspond to bound states or resonances and are characterized by their energies E_λ and by their reduced width amplitudes γ_i^λ. When $N = 1$, i.e., in the single-pole approximation, the R-matrix theory is equivalent to the Breit-Wigner approximation.

The R-matrix parameters, or "calculable" parameters $(E_\lambda, \gamma_i^\lambda)$, depend on the channel radius. They are related to the "observed" parameters (resonance energy E_r and reduced widths $\tilde{\gamma}_i$) by well-known transformations [18]. In practice, the observed parameters, which can be directly compared to experiment, are used as input data to the fit, and then converted to R-matrix parameters to be used in Eq. (3). They do not depend on the channel radius. The partial width Γ_i of pole λ in channel i is related to the observed reduced width $\tilde{\gamma}_i^2$ by

$$\Gamma_i = 2\tilde{\gamma}_i^2 P_\ell(E_r), \tag{4}$$

where $P_\ell(E)$ is the Coulomb penetration factor in angular momentum ℓ. The dimensionless reduced widths are defined as

$$\theta_i^2 = \tilde{\gamma}_i^2 / \gamma_W^2, \tag{5}$$

where $\gamma_W^2 = 3\hbar^2/2\mu_i a^2$ is the Wigner limit (and for the sake of clarity we drop index λ). These quantities are known to provide information on the cluster structure of a state. Small values (i.e., of the order of 1% or less) are typical of compact states. In contrast, large values (typically $\theta_i^2 \gtrsim 10\%$) correspond to deformed states, or, in the traditional terminology of nucleon+nucleus systems, to single-particle states.

The collision matrix $\boldsymbol{U}$, which provides the cross section, is obtained from the R-matrix parameters in various partial waves $J\pi$ (see Refs. [16,17]). In the present work, the R matrix and the collision matrix are of dimension two: elements R_{11} and U_{11} are associated with the $^8\text{Li} + p$ elastic channel, whereas elements R_{12} and U_{12} determine the ^{8}Li(p, α)^{5}He cross section (with both matrices being symmetrical). The transfer cross section at the center-of-mass (c.m.) angle θ is obtained from

$$\frac{d\sigma_t}{d\Omega}(E,\theta) = \frac{1}{10k^2} \sum_j B_j(E) P_j(\cos\theta), \tag{6}$$

where k is the wave number in the $^8\text{Li} + p$ entrance channel, and $B_j(E)$ are the anisotropy coefficients, directly deduced from the collision matrices in the different partial waves (see Sec. VIII of Ref. [16]). In Eq. (6), the energy and angular dependencies have been factorized through the Legendre polynomials $P_j(\cos\theta)$. The term with $j = 0$ is dominant at low energies and corresponds to the isotropic component. The integrated cross section only involves $B_0(E)$. For a transfer reaction the c.m. angle θ is related to the laboratory angle θ_{lab} by well-known formulas [19]. Unless specified otherwise, all energies are defined in the c.m. frame.

B. Application to the ^{8}Li(p, α)^{5}He reaction

In the literature, the spectrum of ^{9}Be is poorly known at high excitation energies [6,7,13]. In particular, the partial widths, which determine the cross section at low energies, are not available. The currently adopted data [13] are summed up in Table I.

The ^{8}Li(p, α)^{5}He reaction involves three particles in the exit channel. However, as suggested by simulations (see

TABLE II. Resonance properties (with energies in MeV, widths in keV, and dimensionless reduced widths in percent). The relative uncertainties on the reduced widths are identical to those of the total widths.

Present							Literature [13]		
E_r	J^π	(I,ℓ)	Γ_p	Γ_α	θ_p^2	θ_α^2	E_r	J^π	Γ
-0.22	$5/2^+$	$(5/2, 0)$	550 ± 100[a]	41 ± 4	19.7	0.3	-0.22	$(5/2^+)$	41 ± 4
0.38 ± 0.08	$5/2^-$	$(5/2, 1)$	5 ± 1	180 ± 50	2.7	1.4	0.40	$(5/2)^-$	200
0.61 ± 0.03	$7/2^+$	$(5/2, 2)$	1.4 ± 0.4	39 ± 15	3.5	0.3	0.605	$(7/2)^+$	47
1.69 ± 0.03	$5/2^+$	$(5/2, 0)$	250 ± 50	430 ± 80	4.3	3.1	1.69		
1.76 ± 0.04	$7/2^+$	$(3/2, 2)$	70 ± 13	420 ± 80	8.4	3.5	1.76	$(5/2^-)$[b]	300 ± 100

[a]Reduced proton width $\tilde{\gamma}_p^2$.
[b]Tentatively assigned to isospin $T = 3/2$.

Sec. II), assuming a sequential two-body $\alpha + {}^5$He decay is a reasonable approximation and allows a standard two-body treatment of the data. In addition, although ${}^7\text{Li} + d$ ($Q = -0.19$ MeV) and ${}^8\text{Be} + n$ ($Q = -15.22$ MeV) channels are open at threshold, these exit channels can be neglected since we are looking for states with a dominant ${}^8\text{Li} + p$ or $\alpha + {}^5$He structure.

In the entrance channel, the channel spin I is $I = 3/2$ or $I = 5/2$, and several orbital-momentum values ℓ are consistent with spin couplings. In the present fit, however, we take a single set of (I, ℓ) values for each resonance. The orbital momentum ℓ is chosen as the minimum value, according to barrier-penetration effects. The channel spins I are determined to optimize the fit.

The R-matrix fits were performed at $\theta_{\text{lab}} = 13.5^\circ$, where the experimental data cover the whole energy range, from 0.2 to 2.1 MeV. The parameters are given in Table II, and the corresponding fit is shown in Fig. 7. The c.m. angle θ depends on energy and is around 160° in the considered energy range. The experimental energy resolution is taken into account by folding the R-matrix results with a Gaussian distribution. The channel radius is taken as $a = 5$ fm, but the χ^2 values

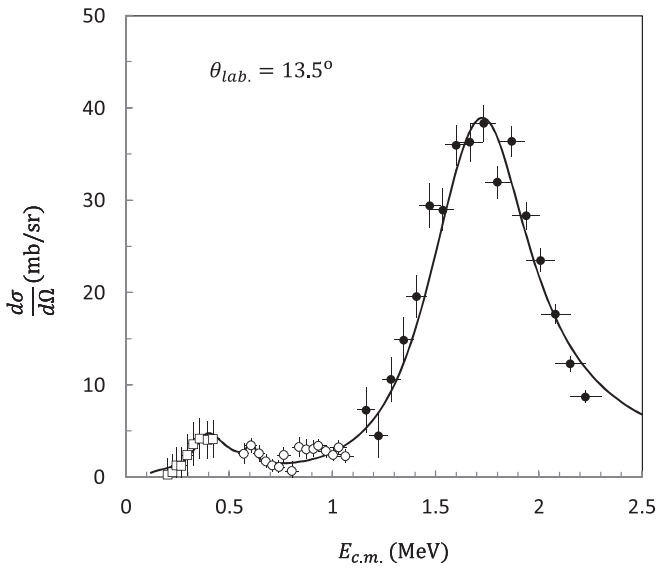

FIG. 7. ${}^8\text{Li}(p,\alpha){}^5\text{He}$ differential cross sections at $\theta_{\text{lab}} = 13.5^\circ$, with the R-matrix fit (solid line). The data are presented as in Fig. 6.

are virtually insensitive to that choice. At the minimum, the reduced χ^2 is $\chi^2/N = 0.46$ (where $N = 90$ is the number of data points) when all data points are included and 0.76 when the average procedure is applied (see Fig. 6). To determine the χ^2, the error bars on energy have been converted into cross-section error bars [20].

Let us first discuss the low-energy part of the cross section. Above threshold, the lowest experimental resonance (see Table I) presents an isospin $T = 3/2$ [14]. The 14.302- and 16.975-MeV states are not expected to play a role. Although charge symmetry reduces the expected contribution of the 16.975-MeV resonance to the cross section, the experimental upper limit on the probability for this state to decay by α emission is 75% [13], and therefore a significant contribution cannot be ruled out. The experimental data of Fig. 7 clearly show two peaks at low energies (near 0.4 and 0.6 MeV). The low-energy dependence can be reproduced by including the subthreshold state ($E_r = -0.22$ MeV) and two resonances at 0.38 and 0.61 MeV. These three $T = 1/2$ states are known in the literature [13], but their partial widths were not measured. For the -0.22-MeV state, we fixed the energy to the experimental value as the χ^2 is weakly sensitive to its value. It is, however, rather sensitive to the proton reduced width, which is found as $\theta_p^2 = (20 \pm 2)\%$. The energy and width of the two other states are in remarkable agreement with the literature values. The tentative spins $5/2^-$ and $7/2^+$ are confirmed by the present analysis. As expected from Coulomb effects, the proton widths are small, and the total widths are essentially defined in the α channel.

As discussed previously, the present data show evidence for a broad peak near $E_{\text{c.m.}} \approx 1.7$ MeV. Owing to its large amplitude, this peak can be fitted only by assuming two overlapping resonances. The energies (1.69 and 1.76 MeV) are consistent with known spectroscopic properties of ^{9}Be. For the state at $E_{\text{cm}} = 1.69$ MeV, we suggest a $5/2^+$ assignment, which corresponds to an s wave. No information is available in the literature about the width of this state. The second level ($E_{\text{cm}} = 1.76$ MeV) has an energy and total width consistent with previous data. However, its tentative assignment to an isospin $T = 3/2$ state suggests that this state would be populated less than a $T = 1/2$ state with the same quantum numbers. The existence of a broad structure near $E_x = 18.6$ MeV in ^{9}Be has been already suggested by a previous ${}^7\text{Li}(d,\alpha){}^5\text{He}$ experiment [21], and it is consistent with the overlapping states observed in the present experiment.

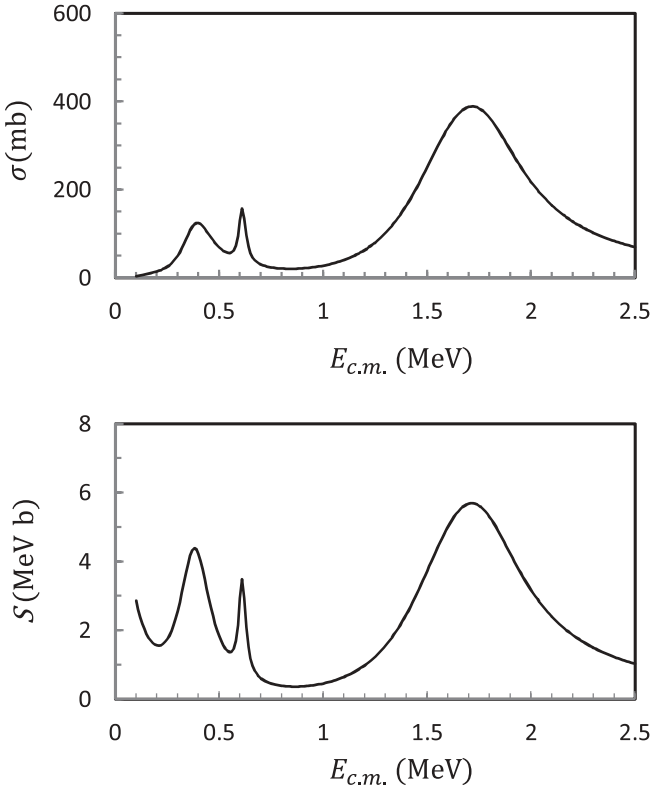

FIG. 8. Integrated cross section (upper panel) and S factor (lower panel) obtained with the R-matrix parameters of Table II.

Partial data have been obtained at $\theta_{\rm lab} = 10.5^\circ$ and 18.5°, with a beam energy of 19.0 MeV only. They also show evidence for a broad structure near 1.7 MeV and suggest an isotropic dependence of the cross section, in agreement with a dominant s-wave contribution. However, owing to the lower statistics, and to the limited energy range, these data were not included in the R-matrix analysis.

C. Astrophysical reaction rate

In Fig. 8, we present the integrated cross section, as well as the corresponding S factor, for the ^{8}Li$(p,\alpha)^5$He reaction. These curves have been obtained from the R-matrix parameters of Table II without any energy convolution. As expected, the peaks are more visible, in particular the narrow $7/2^+$ resonance at 0.61 MeV.

In inhomogeneous Big Bang models [22] and in r-process nucleosynthesis occurring in type II supernovae [23], the ^{8}Li$(p,\alpha)^5$He reaction may compete with the ^{8}Li$(\alpha,n)^{11}$B reaction, which is the starting point for the production of $A \geqslant 12$ elements. A high ^{8}Li$(p,\alpha)^5$He rate would destroy ^{8}Li and make the ^{8}Li$(\alpha,n)^{11}$B reaction less efficient. The present cross-section measurement, performed over a wide energy range, makes it possible to calculate the reaction rate.

The reaction rate contains resonant and nonresonant contributions and has been computed by a numerical integration involving the theoretical cross section of Fig. 8. In order to simplify the presentation, this rate is presented here in an analytical format. It is obtained by approximating the resonant contributions, due to the 0.38- and 0.61-MeV resonances (but the known state at 0.087 MeV is not included since its partial α width is not known), by standard resonant reaction rates [24]. Then, subtracting this resonant rate from the total numerical calculation, we fit the remaining part by using a nonresonant parametrization. Between $T_9 = 0.1$ and $T_9 = 5$, the numerical rate (in cm^3 mol^{-1} s^{-1}) is therefore approximated by

$$\begin{aligned} N_A\langle\sigma v\rangle = {} & 5.36\times10^8 T_9^{-3/2}\,\exp(-4.41/T_9) \\ & + 1.99\times10^8 T_9^{-3/2}\,\exp(-7.08/T_9) \\ & + 5.85\times10^{10} T_9^{-2/3}\,\exp\left(-8.50/T_9^{1/3}\right) \\ & \times\left(1 - 1.70\,T_9 + 0.849\,T_9^2 - 0.175\,T_9^3\right. \\ & \left. + 1.62\times10^{-2}\,T_9^4 - 5.60\times10^{-4}\,T_9^5\right), \end{aligned} \quad (7)$$

where T_9 is the temperature expressed in 10^9 K and N_A is Avogadro's number. The first two terms correspond to the resonant rate (0.38- and 0.61-MeV resonances). The third term is associated with the nonresonant contribution and dominates the rate below $T_9 \approx 0.5$. In this temperature range, our rate is slightly larger than the values provided in Ref. [12], which include a contribution from the 0.087-MeV resonance. It is however smaller (by a factor of 2–9) at higher temperatures due to the different treatment of the resonant contribution. Notice that, strictly speaking, the third term of Eq. (7) is not a nonresonant contribution since it stems from the difference between the total and resonant rates, but it represents a standard and accurate parametrization of the numerical rate. Therefore only the total rate should be considered as meaningful.

As mentioned above, the ^{8}Li$(p,\alpha)^5$He reaction may compete with the ^{8}Li$(\alpha,n)^{11}$B reaction. Although the ^{8}Li$(\alpha,n)^{11}$B cross section has been measured by several groups (see Ref. [10] and references therein) there is still a significant discrepancy between the measurements (see, for example, Fig. 4 of Ref. [25]). In particular, the exclusive data of Ishiyama *et al.* [26] are lower than the other measurements. The determination of the reaction rate requires a numerical integration over the Gamow window [27]. For the ^{8}Li$(p,\alpha)^5$He reaction, we use the present R-matrix fit (Fig. 8) to determine the rate [24]. However, the existing data on ^{8}Li$(\alpha,n)^{11}$B (and the absence of

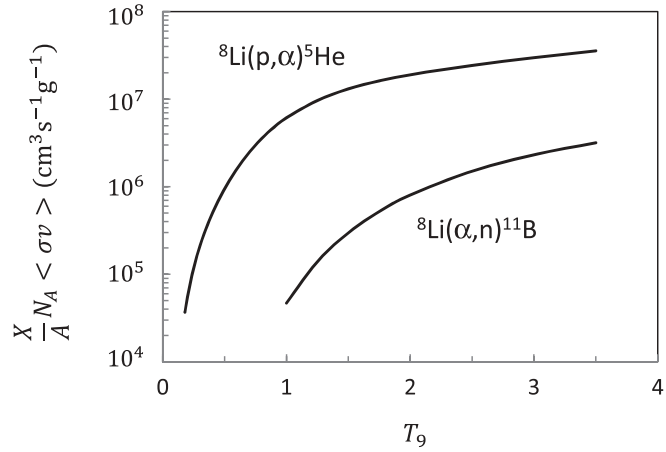

FIG. 9. ^{8}Li$(p,\alpha)^5$He and ^{8}Li$(\alpha,n)^{11}$B reaction rates multiplied by the proton and α mass fractions (see text).

an extrapolation down to zero energy) do not allow an accurate determination of the reaction rate at high temperatures (with typical temperatures in Big Bang nucleosynthesis being of the order of $T_9 \lesssim 0.7$). We have therefore used the analytical parametrization of Gu *et al.* [28] as a first estimate.

To compare two reaction rates involving different entrance channels, we need to include the proton and α mass fractions X_p and X_α [24]. These quantities are necessary to determine the lifetime of a nucleus. In this exploratory work, we take the standard values of the Big Bang, i.e., $X_p = 0.75$ and $X_\alpha = 0.25$. The quantities $N_A\langle\sigma v\rangle X_i/A_i$ are displayed in Fig. 9, which shows that the ^{8}Li$(p,\alpha)^5$He reaction is significantly faster than ^{8}Li$(\alpha,n)^{11}$B at high temperatures. The ^{8}Li$(\alpha,n)^{11}$B data of Ishiyama *et al.* [26] would make this difference still larger.

IV. CONCLUSION AND OUTLOOK

In this work we have studied the ^{8}Li$(p,\alpha)^5$He reaction in reverse kinematics, using an intense ^{8}Li radioactive beam. The goal was twofold: to analyze the properties of ^{9}Be near the proton threshold and to estimate the reaction rate for astrophysical applications. The experiment covered a wide energy range ($E_{\text{c.m.}}$ between 0.2 and 2.1 MeV). The present experiment significantly improves the accuracy of previous data [12] taken at a single energy.

Two low-energy resonances ($5/2^-$ at $E_x = 17.298$ MeV and $7/2^+$ at $E_x = 17.493$ MeV), already known in the literature, have been observed. Their energies and spins could be confirmed by the R-matrix fit, and we were also able to extract partial widths for these states.

The ^{8}Li$(p,\alpha)^5$He cross section presents a broad peak near 1.7 MeV which is almost isotropic. This is interpreted, in an R-matrix analysis, as a superposition of two overlapping resonances, one of them being an s wave. A broad peak is also observed in the ^{8}Li$(d,t)^7$Li reaction [29] and increases the reaction rate. Our low-energy data also provide evidence for the role of a subthreshold state in the S factor.

The present data could be extended to a simultaneous measurement of the ^{8}Li$(p,\alpha)^5$He and ^{8}Li$(p,p)^8$Li cross sections. The availability of elastic-scattering data would provide additional constraints on the R-matrix analysis. In addition, it would also populate $T = 3/2$ states, which cannot be accessed in the ^{8}Li$(p,\alpha)^5$He transfer reaction, according to isospin selection rules. Further information on the ^{9}Be structure near the proton threshold could also be obtained by ^{8}Li$(p,p')^8$Li* inelastic data. This technique has been used recently for other nuclei (see, for example, Ref. [30]) and would provide valuable information on the ^{9}Be structure near the proton threshold. A simultaneous study of the three proton-induced reactions is a challenge for future work.

ACKNOWLEDGMENTS

This work was supported by Fundação de Amparo à Pesquisa do Estado de São Paulo (FAPESP) No. 2003/10099-2, No. 2004/07379-6, and No. 2008/09341-7 and by Conselho Nacional de Desenvolvimento Cientifico e Tecnologico (CNPq) and Comissão de Aperfeiçoamento do Ensino Superior (CAPES). We thank Dr. A. Arazi and Dr. A. Pacheco for enlightening discussions.

[1] N. Keeley, N. Alamanos, K. Kemper, and K. Rusek, Prog. Part. Nucl. Phys. **63**, 396 (2009).
[2] C. Bertulani and A. Gade, Phys. Rep. **485**, 195 (2010).
[3] K. Langanke and M. Wiescher, Rep. Prog. Phys. **64**, 1657 (2001).
[4] R. Lichtenthäler *et al.*, Eur. Phys. J. A **25**, 733 (2005).
[5] E. Benjamim *et al.*, Phys. Lett. B **647**, 30 (2007).
[6] J. P. Glickman *et al.*, Phys. Rev. C **43**, 1740 (1991).
[7] S. Dixit *et al.*, Phys. Rev. C **43**, 1758 (1991).
[8] H. Ishiyama *et al.*, AIP Conf. Proc. **1120**, 177 (2009).
[9] J. F. Lara, T. Kajino, and G. J. Mathews, Phys. Rev. D **73**, 083501 (2006).
[10] M. La Cognata *et al.*, J. Phys. G **37**, 105105 (2010).
[11] T. Sasaqui, K. Otsuki, T. Kajino, and G. J. Mathews, Astrophys. J. **645**, 1345 (2006).
[12] F. D. Becchetti *et al.*, Nucl. Phys. A **550**, 507 (1992).
[13] D. R. Tilley, J. H. Kelley, J. L. Godwin, D. J. Millener, J. E. Purcell, C. G. Sheu, and H. R. Weller, Nucl. Phys. A **745**, 155 (2004).
[14] S. W. Kikstra, S. S. Hanna, A. G. M. van Hees, Z. Guo, and C. van der Leun, Nucl. Phys. A **539**, 1 (1992).
[15] E. Fermi, Prog. Theor. Phys. **5**, 570 (1950).
[16] A. M. Lane and R. G. Thomas, Rev. Mod. Phys. **30**, 257 (1958).
[17] P. Descouvemont and D. Baye, Rep. Prog. Phys. **73**, 036301 (2010).
[18] C. R. Brune, Phys. Rev. C **66**, 044611 (2002).
[19] G. Satchler, *Introduction to Nuclear Reactions* (Oxford University Press, New York, 1990).
[20] R. Barlow, in *Statistics, A Guide to the Use of Statistical Methods in the Physical Sciences*, edited by D. J. Sandiford and F. Mandl (Wiley, New York, 1993).
[21] P. Paul and D. Kohler, Phys. Rev. **129**, 2698 (1963).
[22] T. Kajino, G. J. Mathews, and G. M. Fuller, Astrophys. J. **364**, 7 (1990).
[23] M. Terasawa, K. Sumiyoshi, T. Kajino, G. J. Mathews, and I. Tanihata, Astrophys. J. **562**, 470 (2001).
[24] C. Iliadis, *Nuclear Physics of Stars* (Wiley-VCH Verlag, Berlin, 2007).
[25] M. La Cognata *et al.*, Phys. Lett. B **664**, 157 (2008).
[26] H. Ishiyama *et al.*, Phys. Lett. B **640**, 82 (2006).
[27] C. Angulo *et al.*, Nucl. Phys. A **656**, 3 (1999).
[28] X. Gu *et al.*, Phys. Lett. B **343**, 31 (1995).
[29] T. Hashimoto *et al.*, Phys. Lett. B **674**, 276 (2009).
[30] M. G. Pellegriti *et al.*, Phys. Lett. B **659**, 864 (2008).